J Mater Sci: Mater Electron (2016) 27:9870–9876
DOI 10.1007/s10854-016-5055-7

Fabrication of Sm-doped porous In_2O_3 nanotubes and their excellent formaldehyde-sensing properties

Changbai Liu[1] · Xuesong Wang[2] · Feng Xie[3] · Li Liu[2] · Shengping Ruan[1]

Received: 29 February 2016 / Accepted: 22 May 2016 / Published online: 30 May 2016

Abstract Pure and Sm-doped In_2O_3 porous nanotubes have been successfully fabricated by the single-capillary electrospinning method followed by calcination. The as-synthesized porous nanotubes were investigated by X-ray powder diffraction (XRD), energy-dispersive X-ray (EDX), scanning electron microscope (SEM), Raman spectra and X-ray photoelectron spectroscopy (XPS). It can be seen in SEM images that the surface of nanotubes is distributed with numerous pores. Gas sensing investigation reveals that Sm-doped In_2O_3 porous nanotubes possess high-performance formaldehyde sensing properties. The response of gas sensors based on Sm-doped In_2O_3 porous nanotubes was 54.37 towards 100 ppm formaldehyde at 240 °C, which was 5 times larger than that of pure In_2O_3 porous nanotubes (10.87). The response and recovery times to 100 ppm formaldehyde were 9 and 40 s, respectively. Moreover, even at low concentration of 100 ppb formaldehyde, a detectable response of 2.1 can be observed. Furthermore, Sm-doped In_2O_3 porous nanotube gas sensors have excellent selectivity to formaldehyde.

✉ Li Liu
liul99@jlu.edu.cn

[1] College of Electronic Science and Engineering, Jilin University, 130012 Changchun, People's Republic of China

[2] State Key Laboratory of Superhard Materials, College of Physics, Jilin University, 130012 Changchun, People's Republic of China

[3] College of Environment and Resources, Jilin University, 130012 Changchun, People's Republic of China

1 Introduction

Semiconductor oxides have been widely studied in various fields such as lithium storage [1], photosensitization [2] and gas sensor [3]. Gas sensors based on semiconductor oxides have attracted a lot of attentions in recent years duo to their outstanding advantages such as high sensitivity, easy fabrication and low cost [4]. Semiconductor oxide sensors can be applied in the detection of a wide range of target gases, including hydrogen, nitrogen oxide and formaldehyde [5–7]. These gases are widely used in many areas and they are mostly inflammable or poisonous. Take formaldehyde gas as an example, it has become one of the most common indoor air pollutants since it has been extensively used in many construction materials [8]. This compound has been classified as a probable human carcinogen by the International Agency for Research on Cancer and the World Health Organization (WHO) has established a maximum daily dose reference (RfD) of 0.2 $mg{\cdot}kg^{-1}$ per day for this compound [9, 10]. In view of its toxicity and volatility, exposure to formaldehyde is a potential significant risk to human health and therefore the detection of dilute formaldehyde is particularly important [11]. As is known to us, there are some effective methods to improve the performance of semiconductor oxide gas sensors, such as increasing the surface-to-volume ratio [12] and doping foreign elements [13]. For instance, in order to improve gas sensing properties Li et al. [14] synthesized carbon nanofibers which enhanced surface-to-volume ratio. Tang et al. [15] doping SnO_2 into ZnO nanofibers to improve the sensitivity to methanol. Among the variety of appropriate materials, In_2O_3 is by far one of the most frequently used as gas-sensing materials, which is benefit from its stable and nontoxic characteristics [16]. Various one-dimensional (1D) In_2O_3 nanostructures have been used in gas sensors,

such as nanoparticles [17], nanorods [18] and nanotubes [19]. However, the porous In_2O_3 nanotube structure has rarely been reported. Many studies have shown that the contact of the internal/external surfaces of nanotubes can provide more reaction sites, which is very crucial for their gas sensing properties [20]. Moreover, the porous nanotube structure is a more open structure possessing high surface-to-volume ratio, which makes porous In_2O_3 nanotube a candidate to be used as gas sensors [21]. In addition, the gas-sensing properties can be greatly improved by doping foreign elements [22]. Rare earth (RE)-modified oxide compounds have captured widespread attentions in the past decades because of their particular characteristics arising from the 4f-electrons [23]. Sm is one of the RE elements which has already been used to enhance the gas-sensing properties of materials [24]. However, gas sensors based on Sm-doped In_2O_3 porous nanotubes have never been reported before.

In this paper, pure and Sm-doped In_2O_3 porous nanotubes were successfully synthesized via a simple single-capillary electrospinning method. This novel nanostructure provides a larger contact area with the target gas, which is benefit to enhancing its gas-sensing properties. Furthermore, the gas-sensing properties of the as-synthesized materials to formaldehyde were also investigated. The results demonstrate that the gas-sensing properties of porous In_2O_3 nanotubes have been enhanced significantly by doping Sm.

2 Experimental

2.1 Materials

Indium nitrate hydrate ($In(NO_3)_3$, 99.99 %), samarium nitrate ($Sm(NO_3)_3{\cdot}6H_2O$, 99.99 %), N,N-dimethylformamide (DMF, 99.5 %), and ethanol (≥99.7 %) were obtained from Aladdin (China). Poly (vinyl pyrrolidone) (PVP, $M_w = 1{,}300{,}000$) was purchased from Sigma-Aldrich (USA). All the chemical reagents above were analytical grade and used without further purification.

2.2 Synthesis and characterization of pure and Sm-doped In_2O_3 porous nanotubes

Pure and Sm-doped In_2O_3 porous nanotubes were synthesized via a simple single-nozzle electrospinning method. In a typical process to fabricate Sm-doped In_2O_3 porous nanotubes, 0.4 g of $In(NO_3)_3$ and 0.034 g of $Sm(NO_3)_3{\cdot}6H_2O$ was mixed with 2.0 g of DMF and 2.2 g of ethanol. The two mixtures were under magnetic stirring at room temperature for 30 min. Then, the solution was added into 0.5 g of PVP and kept stirring for 12 h. The mixture was ejected from the stainless steel capillary with a voltage of 13 kV. The distance between the capillary and collector was 25 cm. Then the electrospinning non-woven mats were collected and annealed with a rising rate of 17 °C/min from room temperature and kept at 550 °C for 120 min. At last the furnace was self-cooled to room temperature.

Powder X-ray diffraction (XRD) analysis was conducted on PANalytical Empyrean diffractometer with Cu K_α radiation ($\lambda = 1.5406$ Å). Energy-dispersive X-ray (EDX) spectrometry was performed using an FEL XL30ESEM system. Scanning electron microscope (SEM) images were recorded using an FEL XL30ESEM instrument. Raman spectra were measured by a Renishaw invia microscopic confocal spectrometer, laser wavelength is 514.5 nm. X-ray photoelectron spectroscopy (XPS) measurements were carried out on an ESCLAB KMII using Al as the exciting source.

2.3 Fabrication and measurement of gas sensors

The fabrication and measurement of formaldehyde gas sensors based on the as-prepared materials have been described in our previous work [25]. In brief, the gas sensors were fabricated by coating the paste mixed with Sm-doped In_2O_3 porous nanotubes and deionized water in a weight ratio of 100:20 on a ceramic tube, on which a pair of gold electrodes was previously printed. A small spring-like Ni–Cr alloy was inserted into the ceramic tube to form a side-heated gas sensor. The gas sensors were dried in shade until the first measurement.

Gas sensing tests were performed by a CGS-8 intelligent gas-sensing analysis system (Beijing Elite Tech Co., Ltd., China). The sensors were pre-heated at different operating temperatures until the resistances of all the sensors were stable (relative humidity was about 25 % and room temperature was about 25 °C). When testing, a given amount of saturated target vapor was injected into a test chamber (about 3 L in volume) by a microinjector through a rubber plug to obtain desired concentrations. After the sensors resistance values reached new constant values, the test chamber was opened to recover the sensors in air. All the measurements were performed in a laboratory fume hood. The sensors resistance and response values were acquired by the analysis system automatically.

The sensor response is defined as $\beta = R_a/R_g$, where R_a and R_g are the electrical resistance of the sensors in air and in the target gas, respectively. The response and recovery times are defined as the time taken by the sensor to reach 90 % of the total resistance change in the case of adsorption and desorption, respectively.

3 Results and discussion

3.1 Structure and morphological characteristics

The X-ray diffraction (XRD) pattern was examined to analyze the crystallization of the Sm-doped In_2O_3 porous nanotubes. As shown in Fig. 1, all the samples are well-crystallized, the diffraction peaks can be indexed to cubic In_2O_3 (JCPDS No. 71-2795). No additional impurity peaks were detected, this implys that all the samples were of high purity.

Figure 2 displays the energy-dispersive X-ray (EDX) pattern collected from the Sm-doped In_2O_3 porous nanotubes. It is confirmed that the obtained materials were composed of In, O and Sm. The peak of C was derived from the conducting resin during the measurement. The insert table generally reveals the Sm doping level of In_2O_3 porous nanotubes.

The morphology of the pure and Sm-doped In_2O_3 porous nanotubes is shown in Fig. 3. All the porous nanotubes are randomly oriented and have a uniform diameter of 200 nm approximately. Furthermore, all the surfaces of nanotubes are distributed with apparent pores of uniform size, which provide facilitate passages for gas diffusion throughout the whole nanotubes.

Raman spectroscopy is carried out to further investigate the Sm-doped porous In_2O_3 nanotubes. And the typical Raman spectra is showed in Fig. 4. The obvious bands around 303, 363, 493, and 624 cm^{-1} are assigned to phonon related to cubic structured indium oxide [26–28]. Furthermore, XPS spectra are taken to investigate the chemical composition of the samples, and the results as the Fig. 5 shows. It can be seen that the two peaks located at 451.9 and 444.3 eV are indexed to the In3d, which well match the spin–orbit split of cubic In_2O_3 [29]. Figure 5b shows the peaks are at 1087.7 and 1080.3 eV, which are

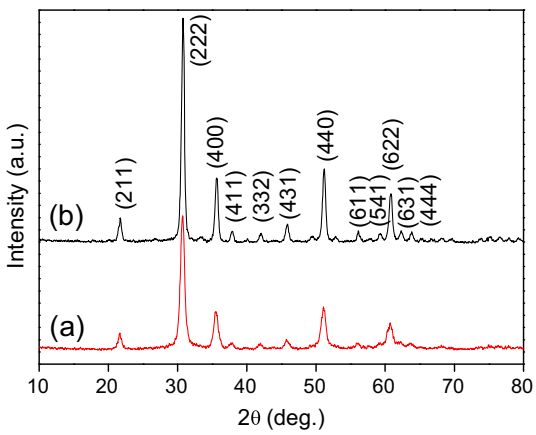

Fig. 1 Full-angle range of XRD patterns of **a** pure and **b** Sm-doped In_2O_3 porous nanotubes

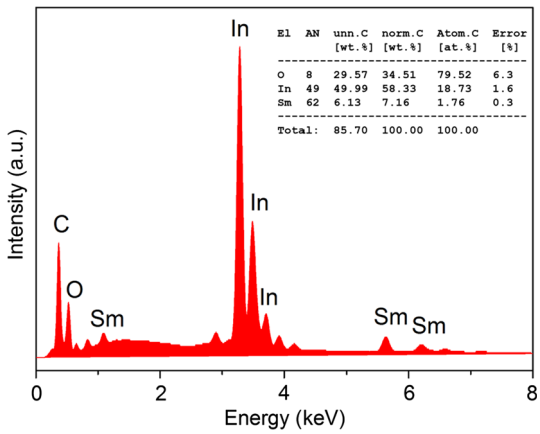

Fig. 2 EDX patterns of Sm-doped In_2O_3 porous nanotubes

assigned to Sm^{3+}. This indicates the formation of Sm_2O_3 nanostructure [30]. The observed XPS profile strongly supports the existences of In_2O_3 and Sm_2O_3.

3.2 Gas-sensing properties of Sm-doped In_2O_3 porous nanotubes

To examine the gas-sensing properties of pure and Sm-doped In_2O_3 porous nanotubes, gas sensors based on pure and Sm-doped In_2O_3 porous nanotubes were manufactured. As is known to all, gas sensors have an optimum operating temperature. Aiming to find out the optimum temperature, the sensors were measured at temperatures ranged from 200 to 280 °C to 100 ppm formaldehyde. From in Fig. 6 that the sensors approached the maximum response at 240 °C and decreased quickly with the increase of the operating temperature. This volcano-shaped temperature dependence of the sensitivity can be explained as below. The reaction rate between the adsorbed oxygen species and formaldehyde molecule is slow at a low temperature, leading to a low sensitivity. When the operating temperature increased too much, some adsorbed gas molecules may escape before their reaction due to their enhanced activation, thus the response will decrease corresponding. When the operating temperature reaches the optimum value, the adsorption and desorption rates of formaldehyde and oxygen species achieve a balance, resulting in the maximum response at 240 °C [21]. Therefore, 240 °C is defined as the optimum operating temperature. Moreover, Sm-doped In_2O_3 porous nanotube sensors showed an excellent response of 54.37, which was about 5 times larger than that of pure In_2O_3 porous nanotube sensors (10.87) to 100 ppm of formaldehyde at 240 °C, indicating the Sm dopant increases the response to formaldehyde significantly.

The response curves of Sm-doped In_2O_3 porous nanotube sensors to different concentrations of formaldehyde at 240 °C are presented in Fig. 7. It shows that the Sm-

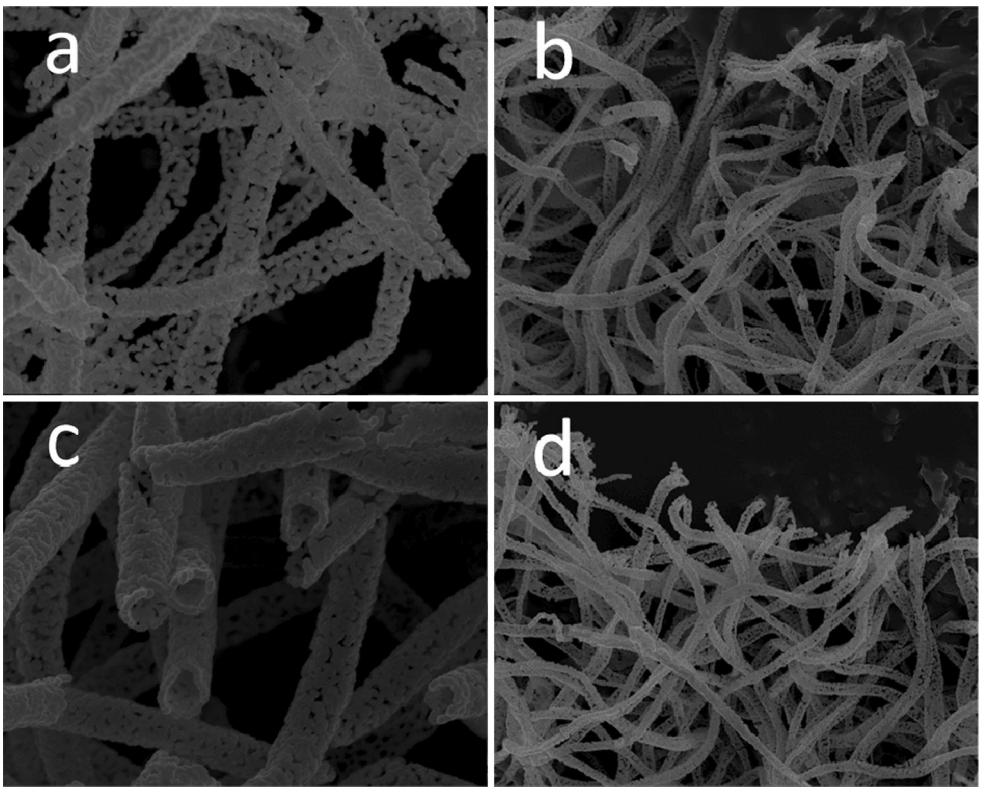

Fig. 3 SEM images of **a**, **b** pure and **c**, **d** Sm-doped In_2O_3 porous nanotubes

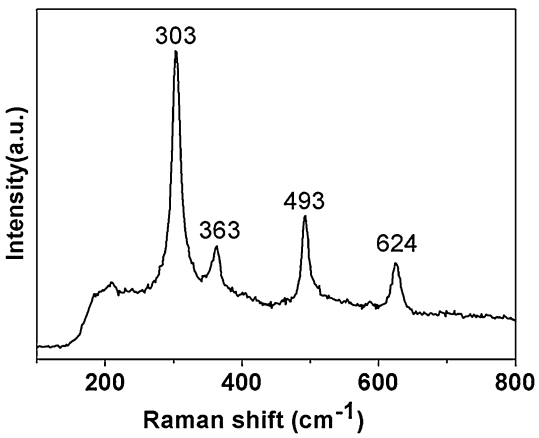

Fig. 4 Raman spectra of Sm-doped In_2O_3 porous nanotubes

doped In_2O_3 porous nanotube sensors have a very wide detection scope. The response of the gas sensors increases rapidly with the increase of formaldehyde concentration. The inset figure represents the calibration curve at low concentrations (0.1–100 ppm), it is apparent that the response of the sensors has a linear relationship with the concentration of formaldehyde. The most important factor in the application of gas sensors is the lowest detection limit concentration. In the gas-sensing test, detectable responses of Sm-doped In_2O_3 porous nanotube sensors can be observed even at 100 ppb of formaldehyde with the value of 2.1. Therefore, the Sm-doped In_2O_3 porous nanotubes are promising materials for the detection of dilute formaldehyde gas in practical application.

The response and recovery characteristic cycle curves of Sm-doped In_2O_3 porous nanotubes to 100 ppm of formaldehyde at 240 °C is displayed in Fig. 8. the response and recovery times are about 9 and 40 s, respectively. The fast response and recovery speed may be due to the excellent porous nanotube structure, which is benefit to the transfer of oxygen and formaldehyde molecules. There are no major changes in the response and recovery times for the four cycles, which indicates the repeatability and stability of Sm-doped In_2O_3 porous nanotubes.

The selectivity to detect a target gas is very important for gas sensors in practical use. Figure 9 shows the excellent selectivity of Sm-doped In_2O_3 porous nanotubes towards a variety of common gases, such as formaldehyde, hydrogen sulfide, ethanol, toluene, carbon monoxide, butane, hydrogen and ammonia. It is clear to see that Sm-doped In_2O_3 porous nanotubes exhibit less sensitivity to other gases, but much higher response to formaldehyde at the same concentrations.

To further illustrate the excellent gas-sensing properties of the as-synthesized materials to formaldehyde, we compared the porous Sm-doped In_2O_3 nanotubes with several

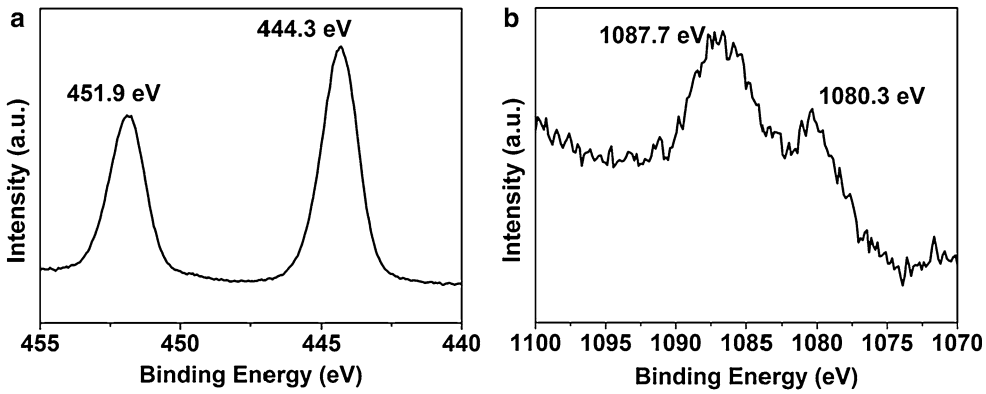

Fig. 5 XPS spectrums of Sm-doped porous In_2O_3 nanotubes, **a** In3d, **b** Sm3d

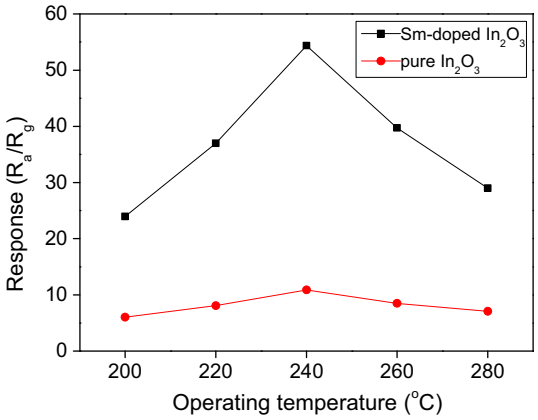

Fig. 6 Responses of pure and Sm-doped In_2O_3 porous nanotubes to 100 ppm formaldehyde at different working temperatures

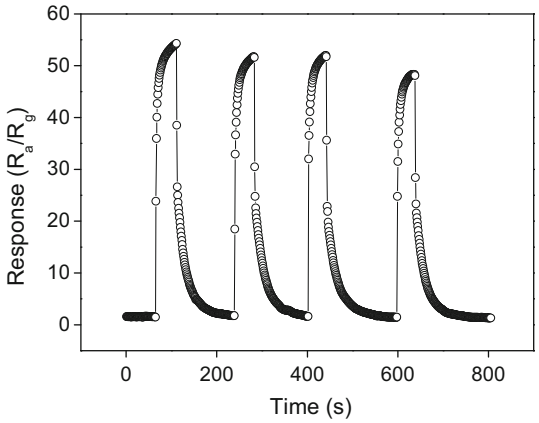

Fig. 8 Response and recovery characteristic cycle curves of Sm-doped In_2O_3 porous nanotube gas sensors to 100 ppm formaldehyde at 240 °C

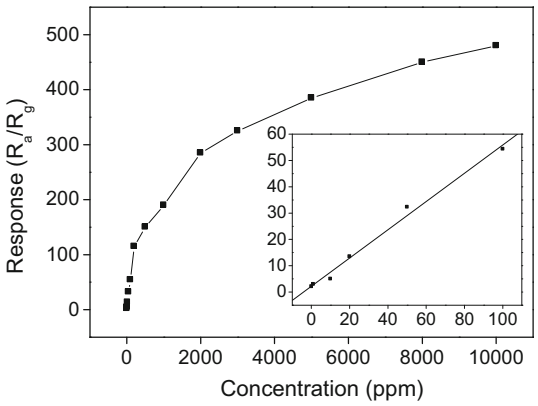

Fig. 7 Response of Sm-doped In_2O_3 porous nanotube gas sensors to different formaldehyde concentrations at 240 °C (The inset presents the calibration curve at low concentrations varying from 0.1 to 100 ppm)

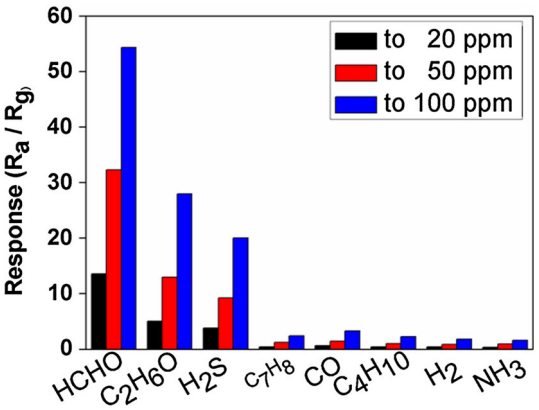

Fig. 9 Sensitivities of Sm-doped In_2O_3 porous nanotube gas sensors to 100 ppm of different gases at 240 °C

previous works and the results ars displayed in Table 1. It can be seen from the comparison that the formaldehyde-sensing properties of the as-obtained porous nanotubes have been significantly improved.

3.3 Gas-sensing mechanisms of Sm-doped In_2O_3 porous nanotubes

The basic principles of semiconductor oxide gas sensors can be explained as the adsorption and desorption of gas

Table 1 Comparison between sensors based on porous Sm-doped In_2O_3 nanotubes and other semiconductors

Gas sensor	Definition of sensitivity	Operation temperature (°C)	Formaldehyde concentration (ppm)	Value of sensitivity (about)	Reference
Sm-In_2O_3	R_a/R_g	240	100	54.37	This work
Ag-In_2O_3/ZnO	R_a/R_g	300	100	8	[31]
SnO_2	R_a/R_g	240	100	25	[32]
Pd-SnO_2	R_a/R_g	150	100	17	[33]
Pt-NiO	R_a/R_g	200	300	5.5	[34]

molecules on the surface of the sensing materials [35]. Briefly, when a sensor is exposed to the air condition, O_2 will be chemisorbed on the surface of In_2O_3 and capture electrons from the materials. Subsequently, the adsorbed O_2 will convert to O_2^-, O^-, and O^{2-}. As a result, the electron density in the conduction band decreases while the resistance of the material increases. However, when a reducing gas such as formaldehyde is introduced, formaldehyde molecules will react with the absorbed oxygen species and then form CO_2 and H_2O. The resistance of the sensor will decrease due to the reaction releases electrons into the conduction band. Thus, a change of the resistance of In_2O_3 is observed. The reactions can be described as the formulas below [36],

$$\begin{aligned} O_2 + e^- &\rightarrow O_2^-, O^-, O^{2-} \\ C_3H_6O + O_2^-, O^-, O^{2-} &\rightarrow CO_2 + H_2O + e^- \end{aligned} \quad (1)$$

Furthermore, the unique porous nanotubes structure is beneficial to enhance the gas sensing properties. It is pretty evident that porosity plays a key role in the efficiency of semiconductor oxide gas sensors [37]. On the one hand, an easier percolation path through the entire porous nanotube must be taken into consideration; on the other hand, more sufficient contact and reaction sites offered by the pores on the nanotube surfaces play another important role. And that will lead to more violent reactions between the adsorbed oxygen species and the target gas, As a result, the change of the sample resistance increases and the response is enhanced [21].

The Sm dopant enhances the gas-sensing properties of In_2O_3 nanotubes significantly. As is known to all, In_2O_3 is an n-type semiconducting oxide [38]. Adachi et al. have demonstrated that Sm_2O_3 is a p-type semiconducting oxide [39]. Numerous studies have shown that when two metal semiconducting oxides with different Fermi levels contact with each other, a heterojunction structure will be formed at the interface of the two oxides [40]. Electrons will flow from the n-type In_2O_3 to p-type Sm_2O_3 while vacancies flow from p-type Sm_2O_3 to n-type In_2O_3. At last the two oxides reach a status of equal Fermi level and a depletion layer is formed at the junction which impedes electronic transmission. As a result, the resistance of Sm-doped In_2O_3 nanotubes in air will increase significantly. However, when a reducing gas such as formaldehyde is introduced, the oxygen adsorbed on the surface of Sm-doped In_2O_3 nanotubes will interact with formaldehyde gas molecules and release electrons into the materials. This leads to a contraction of depletion layer and the improvement of conductivity. The resistance in formaldehyde (R_g) decreases. Therefore the sensitivity of Sm-doped In_2O_3 nanotubes (R_a/R_g) increases. However, excessive dopants will decrease the effective contact areas of nanotubes and target gas, which leads to a decrease of sensitivity [35, 36].

4 Conclusions

In summary, pure and Sm-doped In_2O_3 porous nanotubes were synthesized by the single nozzle electrospinning method and followed calcination treatment. The SEM images display the unique structure of such materials which possesses numerous pores on the nanotube surface. The research of the gas-sensing properties indicated doping Sm to be an efficient method of enhancing the formaldehyde sensing properties of porous In_2O_3 nanotubes. Sm-doped In_2O_3 porous nanotube gas sensors show excellent formaldehyde gas sensitive performance. The response of Sm-doped In_2O_3 porous nanotube gas sensors to 100 ppm formaldehyde is 54.37 at the optimum operating temperature of 240 °C, which is much higher than that of pure In_2O_3 porous nanotubes (response value is 10.78), and the response and recovery times are 9 and 40 s, respectively. The lowest detecting limit to formaldehyde is 100 ppb, and the response value is 2.1. Otherwise, the Sm-doped In_2O_3 porous nanotubes exhibit excellent selectivity towards formaldehyde indicating this material has a good prospect in practical applications.

Acknowledgments The work has been supported by the Jilin Provincial Science and Technology Department (No. 20140204027GX).

References

1. Q. Zhao, L. Ma, Q. Zhang, C. Wang, X. Xu, J. Nanomater. **2015**, 1 (2015). doi:10.1155/2015/850147
2. L.I. Hernández, R. Godin, J.J. Bergkamp et al., J. Phys. Chem. B **117**, 4568 (2013). doi:10.1021/jp3086792
3. X. Li, H. Zhang, C. Feng et al., RSC Adv. **4**, 27552 (2014). doi:10.1039/c4ra03307h
4. Q. Qi, P.-P. Wang, J. Zhao et al., Sens. Actuators B: Chem. **194**, 440 (2014). doi:10.1016/j.snb.2013.12.115
5. Z. Wang, Z. Li, T. Jiang, X. Xu, C. Wang, ACS Appl. Mater. Interfaces **5**, 2013 (2013). doi:10.1021/am3028553
6. J. Gao, L. Wang, K. Kan et al., J. Mater. Chem. A **2**, 949 (2014). doi:10.1039/c3ta13943c
7. P.-J. Yao, J. Wang, Q. Qiao, H.-Y. Du, J. Mater. Sci. **50**, 1338 (2014). doi:10.1007/s10853-014-8694-1
8. A. Chaudhary, S. Hellweg, Environ. Sci. Technol. **48**, 14607 (2014). doi:10.1021/es5045024
9. A. Afkhami, H. Bagheri, T. Madrakian, Desalination **281**, 151 (2011). doi:10.1016/j.desal.2011.07.052
10. A. Afkhami, H. Bagheri, Microchim. Acta **176**, 217 (2011). doi:10.1007/s00604-011-0715-z
11. C. Bosetti, J.K. McLaughlin, R.E. Tarone, E. Pira, C. La Vecchia, Ann. Oncol. **19**, 29 (2007). doi:10.1093/annonc/mdm202
12. T. Guo, Y. Luo, Y. Zhang, Y.-H. Lin, C.-W. Nan, J. Appl. Phys. **116**, 044309 (2014). doi:10.1063/1.4890938
13. C. Zhao, W. Hu, Z. Zhang, J. Zhou, X. Pan, E. Xie, Sens. Actuators B: Chem. **195**, 486 (2014). doi:10.1016/j.snb.2014.01.084
14. W. Li, L.-S. Zhang, Q. Wang et al., J. Mater. Chem. **22**, 15342 (2012). doi:10.1039/c2jm32031b
15. W. Tang, J. Wang, P. Yao, X. Li, Sens. Actuators B: Chem. **192**, 543 (2014). doi:10.1016/j.snb.2013.11.003
16. L xu, B Dong, Y Wang, et al. (2010) Journal of Physical Chemstry C 114: 7
17. L. Wang, X. Xu, Ceram. Int. **41**, 7687 (2015). doi:10.1016/j.ceramint.2015.02.097
18. S. Xu, J. Gao, L. Wang et al., Nanoscale **7**, 14643 (2015). doi:10.1039/c5nr03796d
19. C. Zhao, B. Huang, E. Xie, J. Zhou, Z. Zhang, Sens. Actuators B: Chem. **207**, 313 (2015). doi:10.1016/j.snb.2014.10.087
20. C. Liu, X. Chi, X. Liu, S. Wang, J. Alloy. Compd. **616**, 208 (2014). doi:10.1016/j.jallcom.2014.07.112
21. M. Tiemann, Chem. —Eur. J. **13**, 8376 (2007). doi:10.1002/chem.200700927
22. Y.-B. Zhang, J. Yin, L. Li, L.-X. Zhang, L.-J. Bie, Sens. Actuators B: Chem. **202**, 500 (2014). doi:10.1016/j.snb.2014.05.111
23. H.-Q. Wang, M. Batentschuk, A. Osvet, L. Pinna, C.J. Brabec, Adv. Mater. **23**, 2675 (2011). doi:10.1002/adma.201100511
24. H.T. Giang, H.T. Duy, P.Q. Ngan et al., Sens. Actuators B: Chem. **158**, 246 (2011). doi:10.1016/j.snb.2011.06.013
25. L. Liu, C. Liu, S. Li et al., Sens. Actuators B: Chem. **177**, 893 (2013). doi:10.1016/j.snb.2012.11.106
26. G.F. Pérez-Sánchez, F. Chávez, D. Cortés-Salinas et al., Vacuum **107**, 236 (2014). doi:10.1016/j.vacuum.2014.02.012
27. L.X. Zhang, Y.C. Zhang, M. Zhang, Mater. Chem. Phys. **118**, 223 (2009). doi:10.1016/j.matchemphys.2009.07.047
28. A. Singhal, S.N. Achary, J. Manjanna, O.D. Jayakumar, R.M. Kadam, A.K. Tyagi, J. Phys. Chem. C **113**, 3600 (2009). doi:10.1016/j.snb.2015.04.083
29. D. Han, P. Song, S. Zhang, H. Zhang, Q. Xu, Q. Wang, Sens. Actuators B: Chem. **216**, 488 (2015). doi:10.1016/j.snb.2015.04.083
30. B.T. Sone, E. Manikandan, A. Gurib-Fakim, M. Maaza, J. Alloy. Compd. **650**, 357 (2015). doi:10.1016/j.jallcom.2015.07.272
31. C. Dong, X. Liu, B. Han, S. Deng, X. Xiao, Y. Wang, Sens. Actuators B: Chem. **224**, 193 (2016). doi:10.1016/j.snb.2015.09.107
32. H. Ren, W. Zhao, L. Wang, S.O. Ryu, C. Gu, J. Alloy. Compd. **653**, 611 (2015). doi:10.1016/j.jallcom.2015.09.065
33. Y. Lin, W. Wei, Y. Li et al., J. Alloy. Compd. **651**, 690 (2015). doi:10.1016/j.jallcom.2015.08.174
34. C. Dong, Q. Li, G. Chen, X. Xiao, Y. Wang, Sens. Actuators B: Chem. **220**, 171 (2015). doi:10.1016/j.snb.2015.05.056
35. H. Shan, C. Liu, L. Liu et al., Sens. Actuators B: Chem. **184**, 243 (2013). doi:10.1016/j.snb.2013.04.088
36. X. Chi, C. Liu, L. Liu et al., Mater. Sci. Semicond. Process. **18**, 160 (2014). doi:10.1016/j.mssp.2013.11.016
37. G.X. Wan, S.Y. Ma, X.W. Sun et al., Mater. Lett. **145**, 48 (2015). doi:10.1016/j.matlet.2015.01.085
38. L. Xu, H. Song, B. Dong, Y. Wang, J. Chen, X. Bai, Inorg. Chem. **49**, 10590 (2010). doi:10.1021/ic101602a
39. G.-Y. Adachi, N. Imanaka, Chem. Rev. **98**, 36 (1998)
40. C. Li, C. Feng, F. Qu et al., Sens. Actuators B: Chem. **207**, 90 (2015). doi:10.1016/j.snb.2014.10.035